Published in final edited form as:

Anal Bioanal Chem. 2005 June ; 382(4): 926–933. doi:10.1007/s00216-005-3195-3.

Metal-enhanced fluorescence using anisotropic silver nanostructures: critical progress to date

Kadir Aslan,

Laboratory for Advanced Medical Plasmonics, Medical Biotechnology Center, Institute of Fluorescence, University of Maryland Biotechnology Institute, 725 West Lombard Street, Baltimore, MD 21201, USA

Joseph R. Lakowicz,

Department of Biochemistry and Molecular Biology, Center for Fluorescence Spectroscopy, Medical Biotechnology Center, University of Maryland School of Medicine, 725 West Lombard Street, Baltimore, MD 21201, USA

Chris D. Geddes

Laboratory for Advanced Medical Plasmonics, Medical Biotechnology Center, Institute of Fluorescence, University of Maryland Biotechnology Institute, 725 West Lombard Street, Baltimore, MD 21201, USA

Department of Biochemistry and Molecular Biology, Center for Fluorescence Spectroscopy, Medical Biotechnology Center, University of Maryland School of Medicine, 725 West Lombard Street, Baltimore, MD 21201, USA

Abstract

In this critical and timely review, the effects of anisotropic silver nanostructures on the emission intensity and photostability of a key fluorophore that is frequently used in many biological assays is examined. The silver nanostructures consist of triangular, rod-like, and fractal-like nanoparticles of silver deposited on conventional glass substrates. The close proximity to silver nanostructures results in greater intensity and photostability of the fluorophore than for fluorophores solely deposited on glass substrates. These new anisotropic silver nanostructure-coated surfaces show much more favorable effects than silver island films or silver colloid-coated substrates. Subsequently, the use of metal-enhanced fluorescence (MEF) for biosensing applications is discussed.

Keywords

Silver nanotriangles; Silver nanorods; Anisotropic nanoparticles; Metal-enhanced fluorescence; Radiative decay engineering; Increased excitation rate

C. D. Geddes, geddes@umbi.umd.edu.

Introduction: metal–fluorophore interactions

Fluorescence detection is the basis of most biological assays in high throughput screening and drug discovery today. Although fluorescence is a highly sensitive technique, there is still a need for reduced detection limits, and/or small copy-number detection. Fluorophore detectability is usually limited by the auto-fluorescence of the samples and/or the photostability of the fluorophores. Fluorescence experiments are typically performed in sample geometries that are large relative to the size of the fluorophores and relative to the absorption and emission wavelengths. In this arrangement the fluorophores radiate into free space. Most of the knowledge and intuition about fluorescence are derived from the spectral properties observed in these free-space conditions.

The concept of modifying the radiative decay rate is unfamiliar to many fluorescence spectroscopists. It is therefore informative to consider the novel spectral effects expected upon increasing the radiative rate. The presence of a nearby metal (m) surface increases the radiative rate by the addition of a new rate Γ_m (Fig. 1, right). In this case, the quantum yield (Q_m) and lifetime (τ_m) of the fluorophore near the metal surface are given by:

$$Q_m = \frac{\Gamma + \Gamma_m}{\Gamma + \Gamma_m + k_{nr}}$$
$$\tau_m = \frac{1}{\Gamma + \Gamma_m + k_{nr}} \quad (1)$$

These equations result in unusual predictions for a fluorophore near a metal surface. As the value of Γ_m increases, the quantum yield increases while the lifetime decreases. To illustrate this point we calculated the lifetime and quantum yield for fluorophores with an assumed natural lifetime τ_N=10 ns, $\Gamma=10^8$ s^{-1} and various values for the non-radiative decay rates and quantum yields. The values of k_{nr} varied from 0 to 9.9×10^7 s^{-1}, resulting in quantum yields of 1.0 to 0.01. Suppose the metal results in increasing values of Γ_m. Since Γ_m is a rate process returning the fluorophore to the ground state, the lifetime decreases as Γ_m becomes comparable and larger than Γ (Fig. 2A, left) [1].

As a result of these calculations, we predicted that the metallic surfaces can create unique fluorophores with increased quantum yields and shorter lifetimes. Figure 2B shows that the presence of a metal surface within close proximity of a fluorophore with low quantum yield (Q_0=0.01) increases its quantum yield approximately tenfold, resulting in brighter emission, while reducing its lifetime tenfold, resulting in an enhanced photostability of the fluorophore due to spending less time in an excited state [1].

In earlier efforts, it was proven experimentally that the presence of nearby spherical silver particles can alter the free-space condition and can result in dramatic spectral changes distinct from those observable in the absence of metallic surfaces [2–4]. Remarkably, the spherical silver particles can increase or decrease the intrinsic radiative decay rates of fluorophores and increase the extent of resonance energy transfer (RET) [2–4]. These effects are attributed to interactions of the excited-state fluorophores with free electrons in the metal, the so-called surface plasmon electrons, which in turn can produce favorable effects

on the fluorophore. The effects of metallic surfaces include fluorophore quenching at short distances (~0–5 nm), spatial variation of the incident light field (~0–15 nm), and changes in the radiative decay rates (~0–20 nm). The use of fluorophore–metal interactions is referred to as radiative decay engineering (RDE) or metal-enhanced fluorescence (MEF).

Anisotropic silver particles are also predicted to enhance the emission of fluorescence, due to the increased local excitation fields around the edges of the particles [1]. Several groups have considered the effects of metallic spheroids on the spectral properties of nearby fluorophores [5–9]. A typical model is shown in Fig. 3A, for a prolate spheroid with an aspect ratio of a/b. The particle is assumed to be a metallic ellipsoid with a fluorophore positioned near the particle. The fluorophore is located outside the particle at a distance r from the center of the spheroid and a distance d from the surface. The fluorophore is located on the major axis and can be oriented parallel or perpendicular to the metallic surface. The presence of a metallic particle can have dramatic effects on the radiative decay rate of a nearby fluorophore. Figure 3b shows the radiative rates expected for a fluorophore at various distances from the surface of a silver particle and for different orientations of the fluorophore transition moment. The most remarkable effect is for a fluorophore perpendicular to the surface of a spheroid with a/b=1.75. In this case the radiative rate can be enhanced by a factor of a thousandfold or greater. The effect is much smaller for a sphere (a/b=1.0), and much smaller for a more elongated spheroid (a/b=3.0) when the optical transition is not in resonance [1].

Overview of preparation of novel silver nanostructures for metal-enhanced fluorescence

For medical and biotechnology applications, such as in diagnostic or microfluidic devices, it would be useful to obtain MEF at desired locations in the measurement device: MEF on demand. In this regard, recent studies on MEF have been reported using two relatively facile methods for deposition of spherical silver nanoparticles onto glass slides [1–4, 10]; in the first method, silver islands are deposited onto a glass substrate, in a random fashion, by reducing a silver salt with subsequent addition of sodium hydroxide, ammonium hydroxide, and glucose solutions, while the glass substrate is immersed in the solution [2]; in the second method, silver colloids that are prepared separately are deposited, in a random fashion, onto glass substrates simply by immersion [10]. While the deposition of silver nanoparticles onto glass substrate employing the former method is completed within 30 min, the latter method requires a relatively longer time. These experimental platforms utilizing both silver island films and silver colloid films have typically resulted in fluorescence intensity enhancements of five-fold to thirtyfold for fluorophore-labeled proteins with an average silver optical density of 0.4 [2, 10].

On the other hand, the preparation of well-defined anisotropic silver nanostructures on planar surfaces requires sophisticated lithographic techniques, and simpler wet-chemical-based synthesis methods are until now, ill-explored.

The two most common lithographic methods are high-resolution lithography and nanosphere lithography (NSL). E-beam lithography (EBL) is a well-known approach to the

nanofabrication of anisotropic silver nanostructures on planar surfaces, which uses magnetic lenses to focus an electron beam to a submicron spot size. The focused e-beam is mastered to directly write a desired pattern onto a resist-coated substrate. The advantages of creating nanostructures using EBL include exact control over the shape and size of the features and the ability to control the inter-feature separation. The primary disadvantage of using EBL for the fabrication of noble metal nanostructures on a surface is that it is a complicated method that involves multiple processes, and it can therefore only be used to create nanostructures over a small area.

NSL, which was pioneered by Van Duyne and colleagues, is another fabrication method that is used to deposit anisotropic silver nanostructures directly onto conventional glass substrates. In this method, first, glass substrates are immersed in a suspension of polystyrene (PS) nanospheres where PS nanospheres self-assemble in a hexagonal close-packed array. The glass substrate is then mounted in a vacuum chamber and silver is deposited through a mask created by the close-packed PS particles [11–13]. The PS particles are removed, leaving the truncated silver tetrahedral nanostructures on the surface. The size of the silver nanostructures and their spacings can be changed by changing the size of the PS nanospheres that are used as the physical mask and by varying the amount of deposited metal. Truncated silver tetrahedral nanostructures created using NSL exhibit a plasmon resonance band that is tunable (>400 nm) simply by changing the size and shape of the nanostructure [11].

In the last few years, there has been a large increase in the synthesis of anisotropic silver and gold nanoparticles in solution related to applications in nanoscience and nanotechnology [14–17]. The most notable preparation methods include surfactant-based seed-mediated growth [15, 18–22], thermal growth [23–25] and photoreduction processes [26]. These methods yield silver and gold nanoparticles in solution with different shapes, such as rods, triangular plates, and cubes. Despite the simplicity of the synthesis of anisotropic silver nanoparticles in solution, the deposition of such nanoparticles on planar surfaces using wet-chemical synthesis has not been fully exploited.

Recently, Taub et al [27] reported the growth of gold nanorods directly on mica using a method based on surfactant-based seed-mediated growth [15]. This technique was introduced as a first step towards alleviating the need for wet-chemical lithography processes. In addition, Wei et al [28] extended this method for gold nanorods to conventional glass substrates.

Analogous to the wet-chemical method that was applied to the growth of gold nanorods on mica, Aslan et al [29] reported the deposition of silver nanorods and silver triangular nanoplates [30] onto glass substrates (Fig. 4). Two methods have been considered for the deposition of silver nanorods and silver triangular nanoplates onto conventional glass substrates. In the first method, which is applicable only to silver nanorods, the silver nanorods were deposited onto APS-coated glass substrates by simply immersing the substrates into the silver nanorod solution. This slow deposition process took several days to complete, and the absorption at 550 nm reached only 20% of that exhibited by the silver nanorods in solution (Fig. 5A) [29]. The change in absorbance at this wavelength was

chosen specifically since silver nanorods have two distinct surface plasmon peaks: 440 and 550 nm. The surface plasmon peak at 440 nm is the transverse plasmon peak, and the peak at 550 nm is the longitudinal plasmon peak. The wavelength where the longitudinal plasmon peak appears is dependent on the length of the silver nanorods; that is, the longer the nanorod, the greater the red-shifted peak appears.

In the second method, which is applicable to both silver triangular nanoplates and silver nanorods, spherical silver seeds (~4 nm) that were chemically attached to the surface were subsequently converted and grown into silver nanorods or silver triangular nanoplates in the presence of a cationic surfactant and silver ions (Fig. 4). The duration of the immersion of silver seed-coated glass substrates in the growth solution determined whether the silver seeds were converted into triangular nanoplates or nanorods. It was found that keeping the glass substrates coated with silver seeds in CTAB solution for between 1 and 3 min resulted in conversion of all the silver spheres into silver triangular nanoplates (80%) and silver nanorods (20%), and that longer than 3 min (up to 10 min) resulted in conversion of all of the silver spheres into rod-like structures. Immersion times of less than 1 min or longer than 10 min did not yield any conversion of the silver spheres [29, 30].

Figure 5B shows the progressive increase in the absorption of the silver nanorods that were grown from the silver seeds. It is noted that the transverse plasmon peak (due to the surface plasmons oscillating along the height of the silver nanorods or along the shorter axis, indicative of mostly spherical shapes) is more dominant at the beginning of the growth process; however, as longer nanorods are formed, the longitudinal plasmon absorption peak becomes more dominant [29]. Silver triangular nanoplates grown on glass substrates also have two distinct surface plasmon peaks at 440 and 550 nm (Fig. 6). The absorption at these wavelengths increased as the loading density, as well as the size of the silver triangles, was increased, with no apparent shift in the absorption maximum, suggesting that the growth process was equilateral [30].

The aspect ratio of the silver nanorods deposited on glass substrates was larger than two (reaching up to ten) with lengths ranging from a few hundred nanometers to a few micrometers, and diameters ranging from a few hundred nanometers to a few micrometers (determined by the height in the AFM image (see Fig. 7A) [29]. The silver triangles were agglomerated and they varied between 100 and 500 nm in size (determined by the height in the AFM image, see Fig. 7B) [30].

Metal-enhanced fluorescence sensing using anisotropic silver nanostructures on planar surfaces

Over the past few years laboratories at the University of Maryland at Baltimore and the University of Maryland Biotechnology Institute have demonstrated the favorable effects that can be obtained for fluorophores in close proximity to silver surfaces, such as enhanced quantum yields, increased excitation rates, and increased fluorophore photostability [1–4, 10].

To test the usefulness of the anisotropic silver nano-structures-coated glass substrates with regard to MEF, the substrates were tested with a fluorophore, Indocyanine green (ICG), which has been approved for use in humans by the Federal Drug Administration. The ICG displays a low quantum yield in solution, ~0.016 [31], making it a good candidate for MEF, since low quantum yield fluorophores result in greater enhancements [1].

For a low loading of the nanorods on the surface (A_{650}=0.10), then a typical fluorescence enhancement of ten can be obtained. However, for higher loadings, (A_{650}=0.48), reproducible enhancements of 50-fold and even greater can be achieved (Fig. 8A). Figure 8B also shows that the spectral characteristics of ICG are maintained on the silver nanorods [29].

For a low loading of the silver triangular nanoplates on the surface (A_{550}=0.03) then a typical fluorescence enhancement of three can be obtained relative to the glass surface (the control sample). However, for higher loadings, (A_{550}=0.08), enhancements of ≈16-fold can be achieved (Fig. 9A). Figure 9B also shows that the spectral characteristics of ICG are maintained on silver triangular nanoplates [30], as previously observed with silver island films [32]. In these geometries, a typical twentyfold enhancement is achieved for ICG [32], but with much higher silver optical densities (A_{420}=0.4) [32].

Previous reports have shown that the lifetimes of the fluorophores in close proximity to silver nanostructures decrease significantly and so the fluorophores become more photostable due to the fact that there is less excited state time for photochemical processes to occur [2, 10, 32]. In this regard, the photostability of ICG–HSA when bound to glass or anisotropic silver nanostructures was studied by Aslan et al [29, 30]. The intensity of ICG–HSA was recorded with continuous illumination at 760 nm. When excited with the same incident power, the fluorescence intensities, when considered on the same intensity scale, decreased more rapidly on the glass (Figs. 10A, 11A) [29, 30]. Alternatively, one can consider the photostability of ICG when the incident intensity is adjusted to result in the same initial signal intensities on silver and glass. In this case (Figs. 10B, 11B), photobleaching is slower on the silver surfaces [29, 30]. The fact that the photobleaching is not accelerated for ICG on silver indicates that the increased intensities on silver are not due to an increased rate of excitation, but are due to a modification in the apparent radiative decay rate of the fluorophore. In this regard, it is worth additionally noting that the fluorescence enhancements observed in Figs. 8A and 9A, and the ratio of integrated areas under the curves in Figs. 10A and 11A, are not due to reflected photons from the silver, but in fact to a modification of the intrinsic emissive rate of the fluorophore [1].

The MEF results in both increased emission intensity and a reduction in fluorophore lifetime (a radiative rate modification) [1–4, 10]. Figure 12 shows the reduction in lifetime on the silver nanorods (Ag) as compared to the unsilvered glass (G). The amplitude-weighted lifetime was found to decrease from 0.484 ns on the unsilvered glass to 0.023 ns on the silver nanorods (Fig. 12, Table 1).

In regard to the emerging use of MEF in sensing applications, the method and protocols presented here could be a useful tool for the simpler and much more rapid production of

silver assay platforms that can be utilized in biotechnological applications, such as in high-throughput screening and drug discovery based on enhanced-fluorescence detection. The anisotropic silver nanostructures that are grown on glass substrates could significantly improve the sensitivity of fluorescence-based biological assays, as compared to both surfaces comprised of silver island films [1–4, 10] and indeed, unsilvered surfaces.

Conclusions

We have reviewed the recent research on the interactions of fluorophore–anisotropic silver nanostructures, that offer enhanced spectral properties of the fluorophores, such as increased quantum yields, increased rates of excitation, energy transfer, and enhanced fluorophore photostability (reduced lifetimes) [1]. Anisotropic silver nanostructures can be deposited on substrates by lithography and wet-chemical synthesis. In our opinion, these fluorophore-silver effects offer unique perspectives in clinical chemistry and in biochemistry, providing improved background suppression, increased detection limits and even localized excitation. MEF is an emerging technology, which is likely to become widespread in the near future throughout fluorescence-based applications of biotechnology, such as clinical sensing.

Acknowledgments

This work was supported by the NIH, GM070929-01.

References

1. Lakowicz JR (2001) Anal Biochem 298:1–24 [PubMed: 11673890]
2. Lakowicz JR, Shen Y, D'Auria S, Malicka J, Fang J, Gryczynski Z, Gryczynski I (2002) Anal Biochem 301:261–277 [PubMed: 11814297]
3. Lakowicz JR, Shen Y, Gryczynski Z, D'Auria S, Gryczynski I (2001) Biochem Biophys Res Commun 286:875–879 [PubMed: 11527380]
4. Gryczynski I, Malicka J, Shen Y, Gryczynski Z, Lakowicz JR (2002) J Phys Chem B 106:2191–2195
5. Gersten J, Nitzan A (1981) J Chem Phys 75:1139–1152
6. Chew H (1987) J Chem Phys 87:1355–1360
7. Philpott MR (1975) J Chem Phys 62(5):1812–1817
8. Chance RR, Prock A, Silbey R (1978) Adv Chem Phys 37:1–65
9. Weitz DA, Garoff S, Gersten JI, Nitzan A (1983) J Chem Phys 78(9):5324–5338
10. Geddes CD, Cao H, Gryczynski I, Gryczynski Z, Fang J, Lakowicz JR (2003) J Phys Chem A 107:3443–3449
11. Jensen TR, Malinsky MD, Haynes CL, Van Duyne RP (2000) J Phys Chem B 104(45):10549–10556
12. Jensen TR, Duval ML, Kelly KL, Lazarides AA, Schatz GC, Van Duyne RP (1999) J Phys Chem B 103(45):9846–9853
13. Frey W, Woods CK, Chilkoti A (2000) Adv Mater 12(20):1515–1519
14. Xia Y, Yang P, Sun Y, Wu Y, Mayers B, Gates B, Yin Y, Kim F, Yan H (2003) Adv Mater 15:353–389
15. Jana NR, Gearheart L, Murphy CJ (2001) Chem Commun 7:617–618
16. Zhu JJ, Liao XH, Zhao XN (2001) Mater Lett 49:91–95
17. Xiong YJ, Xie Y, Du GO (2002) Chem Lett 1:98–99
18. Jana NR, Gearheart L, Murphy CJ (2001) Adv Mater 13:1389–1393

19. Jana NR, Gearheart L, Murphy CJ (2001) Chem Mater 13:2313–2322
20. Murphy CJ, Jana NR (2002) Adv Mater 14:80–82
21. Jana NR, Gearheart L, Obare SO, Murphy CJ (2002) Langmuir 18:922–927
22. Jana NR, Gearheart L, Murphy CJ (2001) J Phys Chem B 105:4065–4067
23. Sun Y, Mayers B, Xia Y (2003) Nano Lett 3:675–679
24. Jin R, Cao C, Hao E, Metraux GS, Schatz GC, Mirkin CA (2003) Nature 42:487–490
25. Callegari A, Tonti D, Chergi MP (2003) Nano Lett 3:1565–1568
26. Maillard M, Huang P, Brus L (2003) Nano Lett 3:1611–1615
27. Taub N, Krichevski O, Markovich G (2003) J Phys Chem B 107:11579–11582
28. Wei Z, Mieszawska AJ, Zamborini FP (2004) Langmuir 20:4322–4326 [PubMed: 15969133]
29. Aslan K, Leonenko Z, Lakowicz JR, Geddes CD (2005) J Phys Chem B 109(8):3157–3162 [PubMed: 16851335]
30. Aslan K, Lakowicz JR, Geddes CD (2005) J Phys Chem B 109:6247–6251 [PubMed: 16851692]
31. Sevick-Muraca EM, Lopez G, Reynolds JS, Troy TL, Hutchinson CL (1997) Photochem Photobiol 66:55–64 [PubMed: 9230705]
32. Malicka J, Gryczynski I, Geddes CD, Lakowicz JR (2003) J Biomed Opt 8(3):472–478 [PubMed: 12880353]

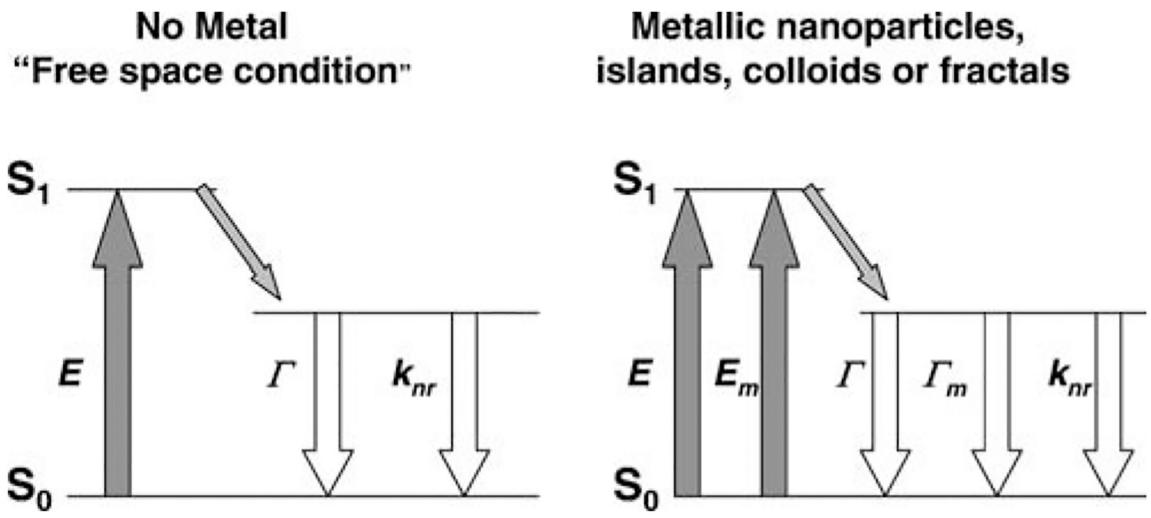

Fig. 1.

Classical Jablonski diagram for the free space condition and the modified form in the presence of metallic particles, islands, colloids, or silver nanostructures. *E*excitation, $E_m$metal-enhanced excitation rate, Γ_m radiative rate in the presence of metal. For our studies, we do not consider the effects of metals on k_{nr}. Adapted from [1]

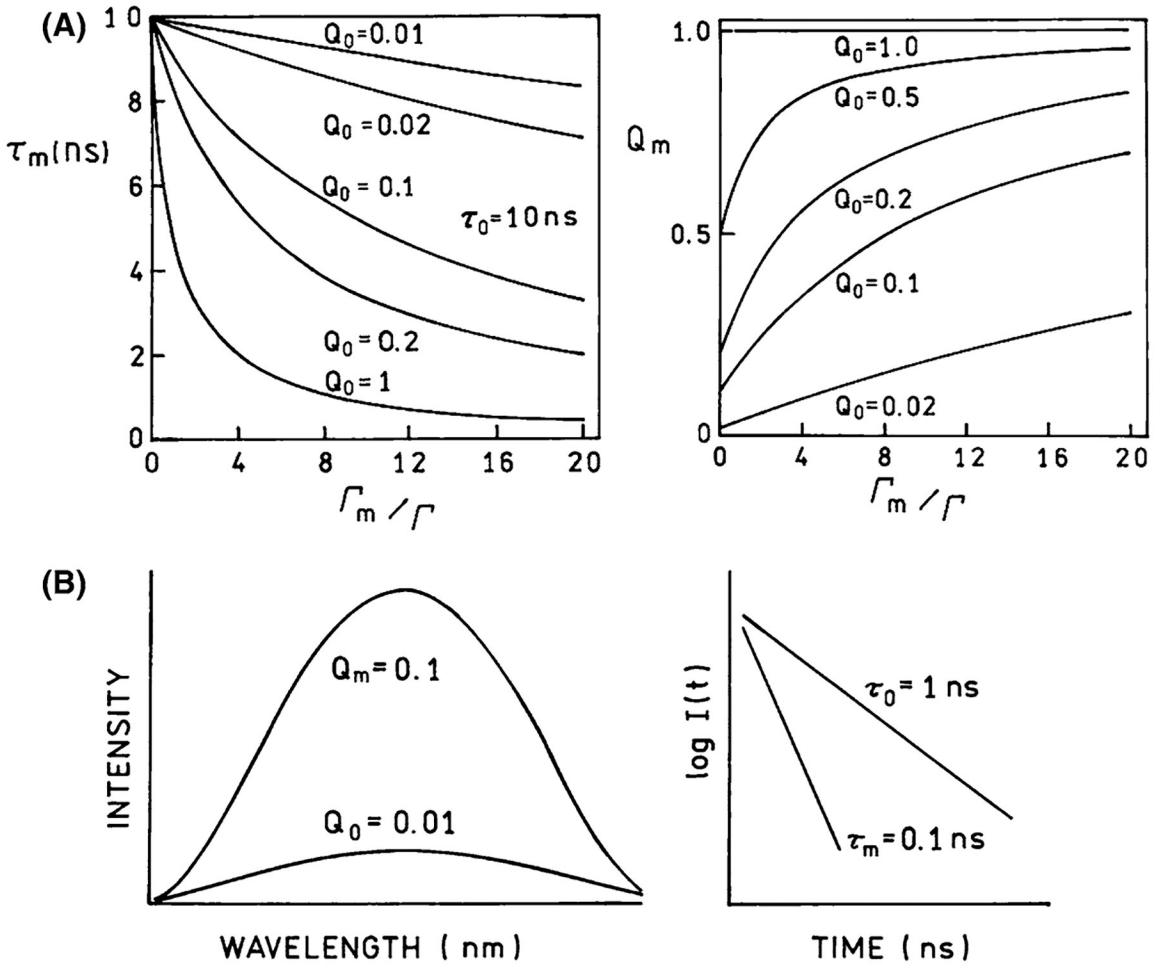

Fig. 2A–B.

A The effect of an increase in radiative decay rate on the lifetime and quantum yield. **B** Metallic surfaces can create unique fluorophores with high quantum yields and short lifetimes. Adapted from [1]

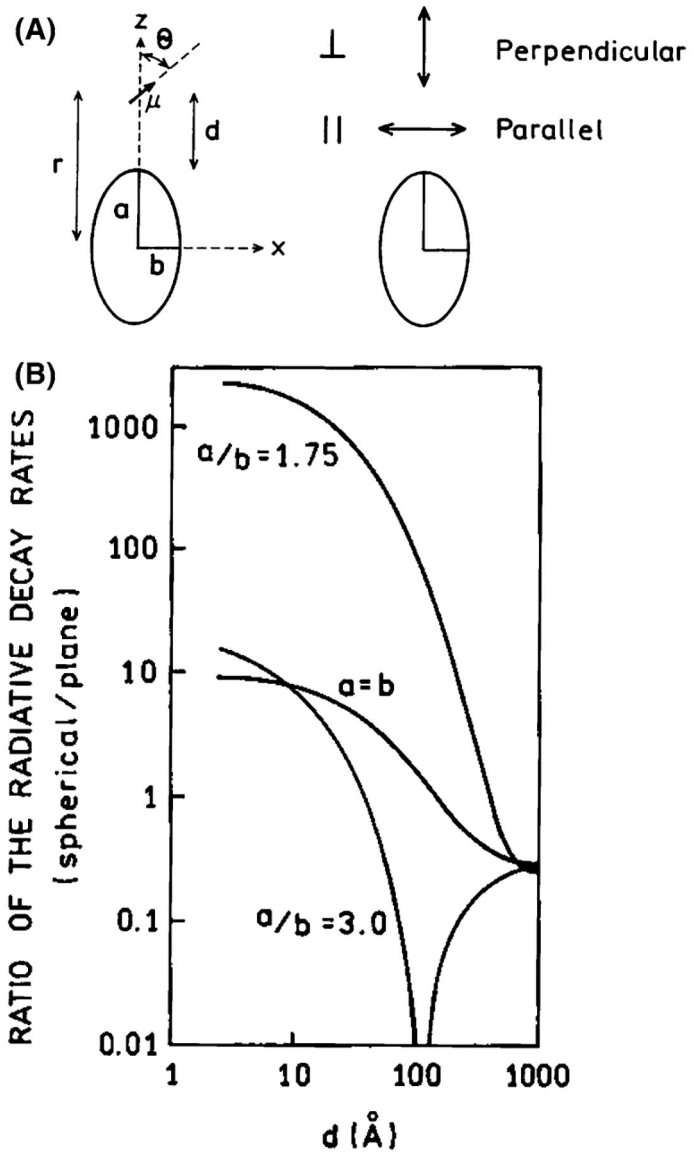

Fig. 3A–B.

A Fluorophore near a metallic spheroid. **B** The resonant frequency of the dye is assumed to be 25,600 cm^{-1}, approximately equal to 391 nm. The volume of the spheroids is equal to that of a sphere with a radius of 200 Å. Adapted from [1]

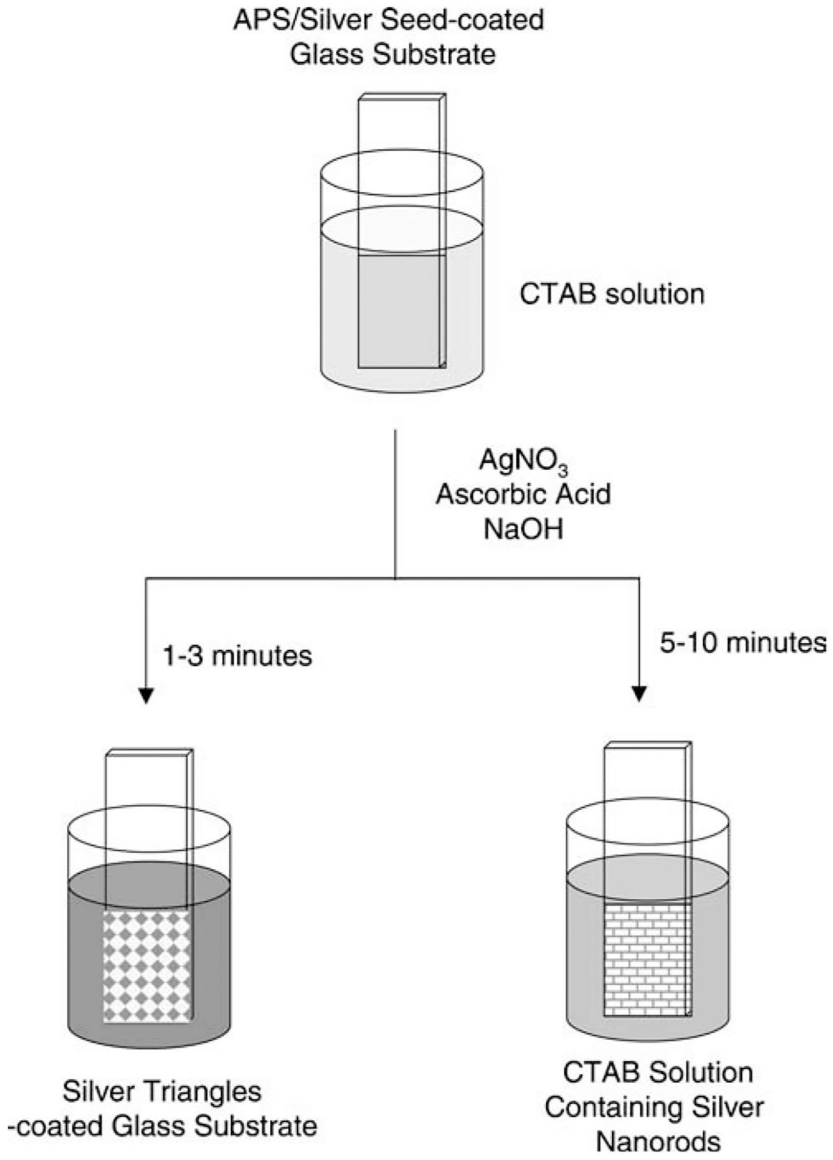

Fig. 4.

Technique for the deposition of silver nanorods and triangular nanoplates on glass substrates

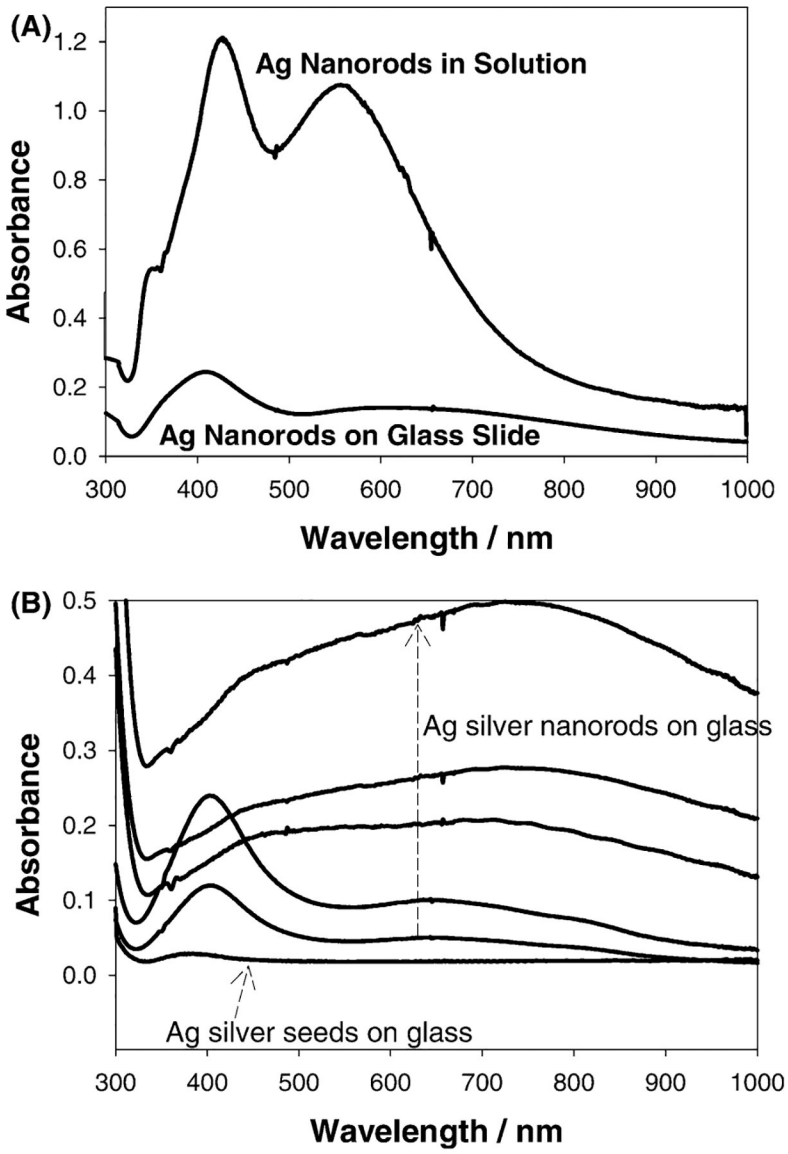

Fig. 5A–B.

A Absorption spectra of silver nanorods in solution and on glass deposited by slow deposition method, **B** absorption spectra of silver nanorods deposited on glass substrates by rapid deposition method. Adapted from [29]

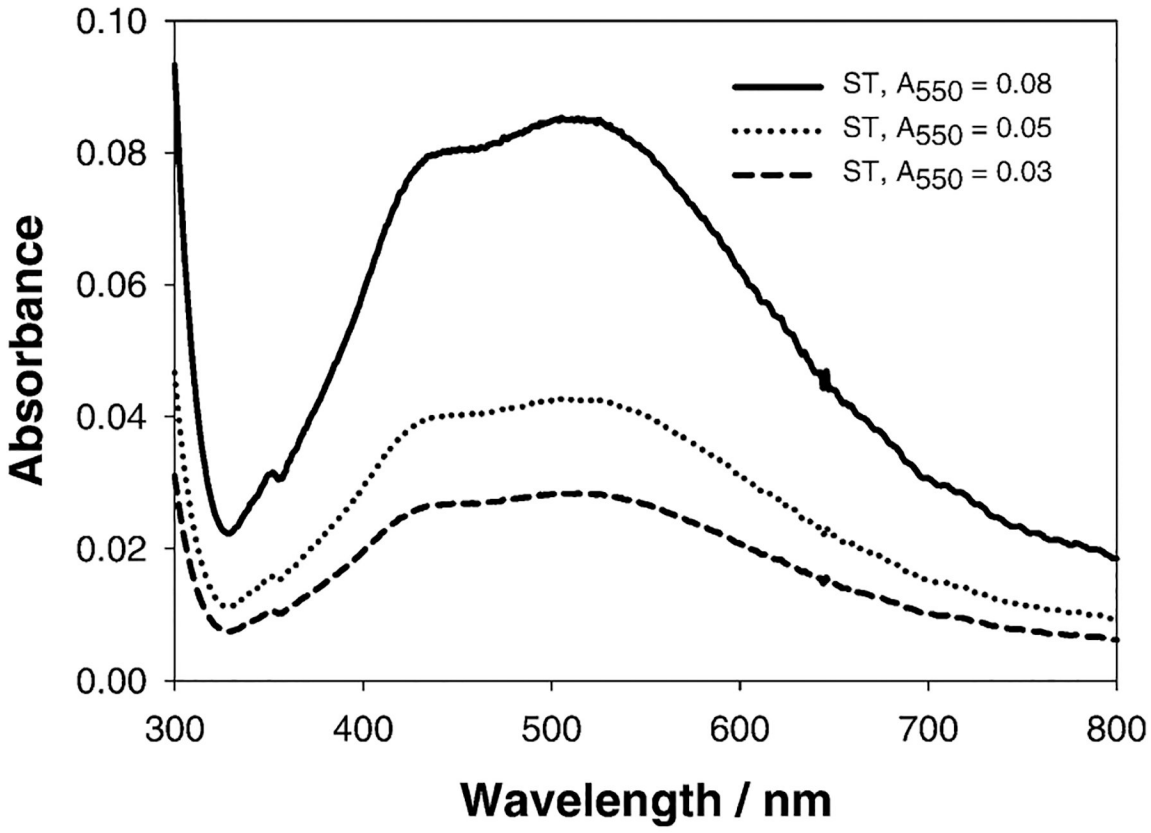

Fig. 6.

Absorption spectra of silver triangular nanoplates deposited on glass substrates by a rapid deposition method. Adapted from [30]

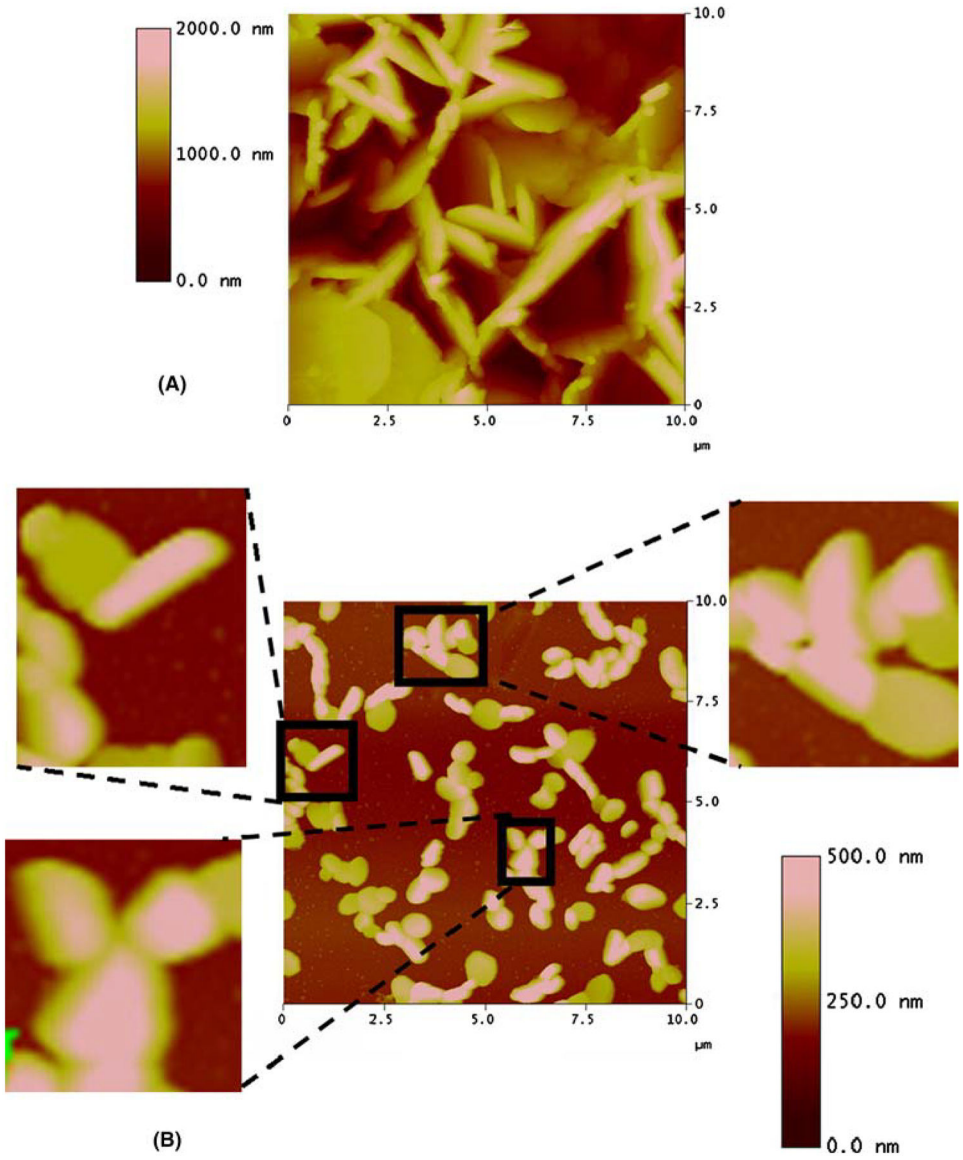

Fig. 7A–B.

A AFM image of silver nanorods deposited on glass substrate, **B** AFM image of silver triangular nanoplates deposited on glass substrate. Adapted from [29, 30]

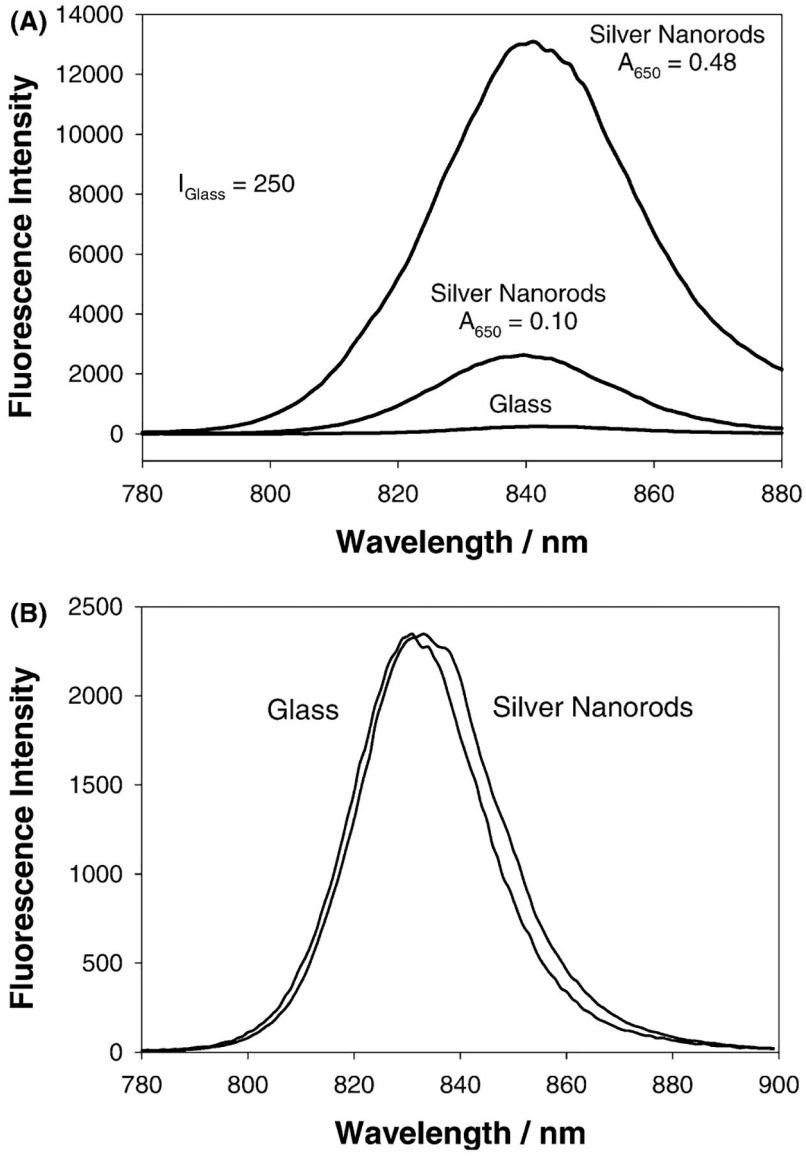

Fig. 8A–B.

A Fluorescence emission intensity of ICG–HSA on silver nanorods with low (A_{650}=0.10) and high loading density (A_{650}=0.48). The arbitrary emission intensity of ICG–HSA on glass is 250. **B** Normalized emission intensities of ICG–HSA on glass and on silver nanorods (A_{650}=0.48), which show identical spectral behavior. Adapted from [29]

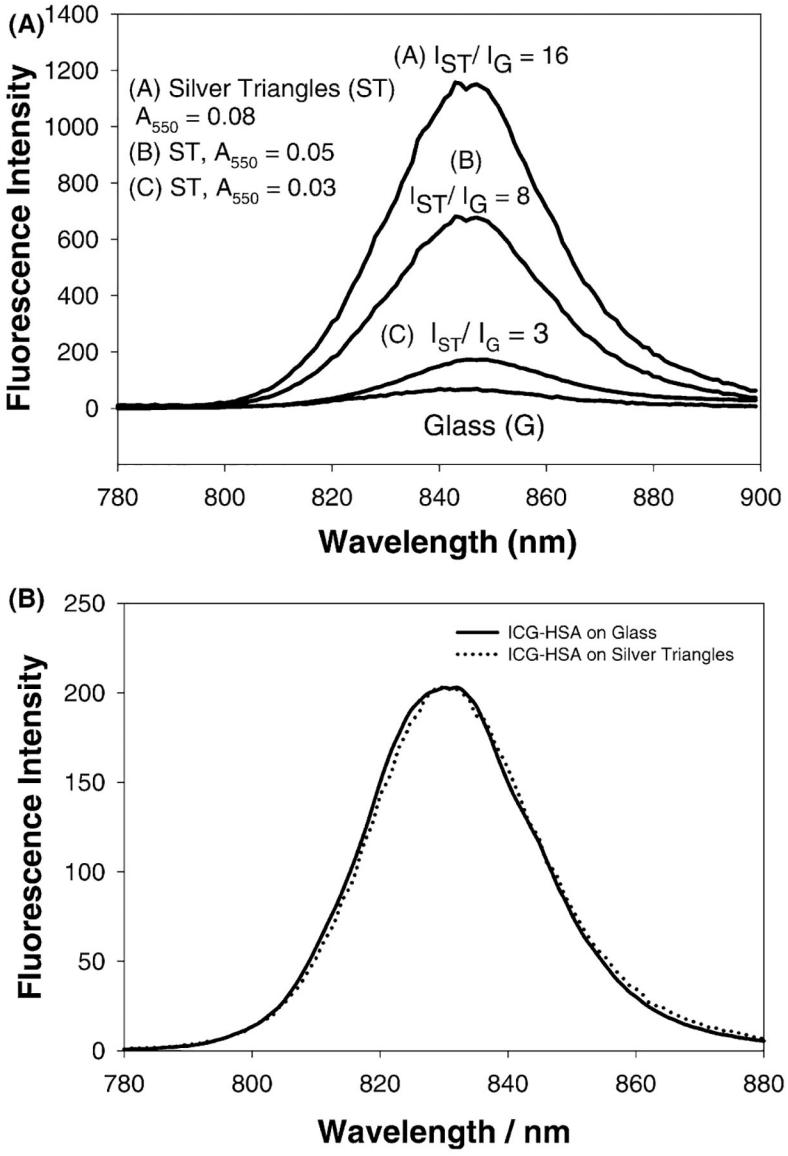

Fig. 9A–B.

A Fluorescence emission intensity of ICG–HSA on silver triangles with different loading densities. The emission intensity of ICG–HSA on glass is 75. **B** Normalized emission intensities of ICG–HSA on glass and on silver nanorods (A_{550}=0.03), which show identical spectral behavior. Adapted from [30]

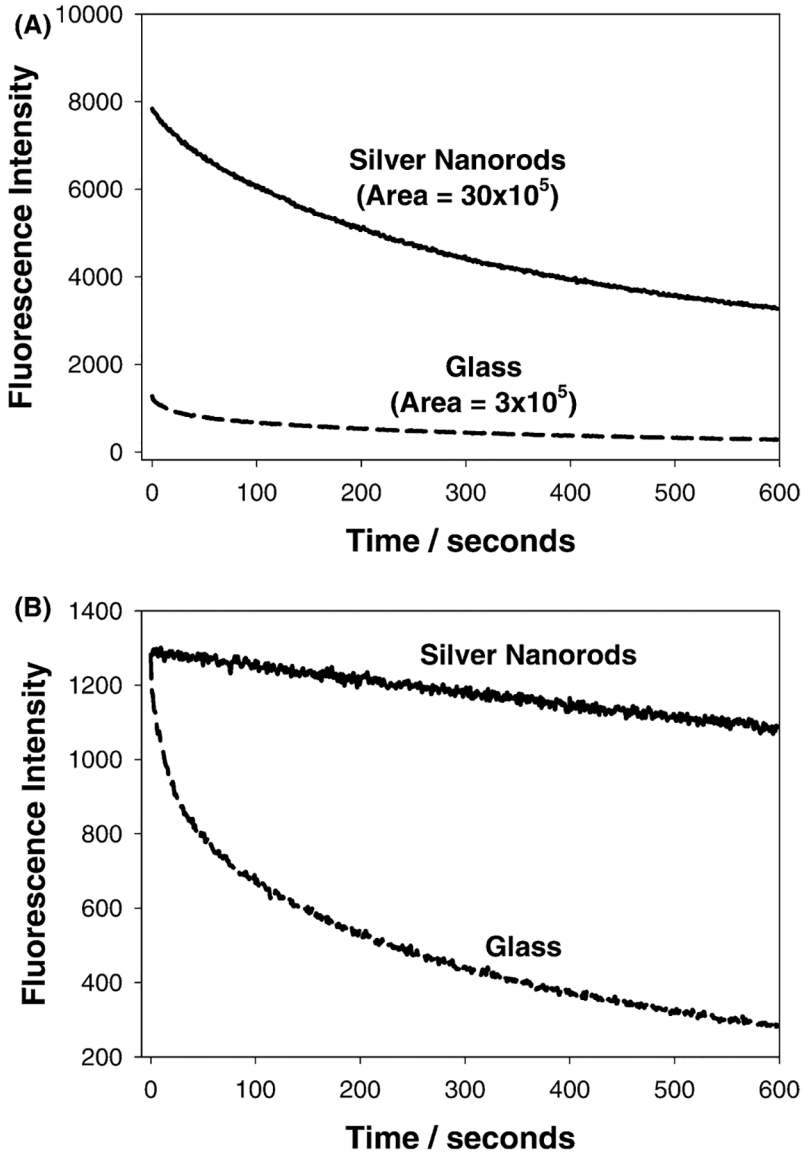

Fig. 10A–B.

A Photostability of ICG–HSA on silver nanorods prepared by the rapid deposition method, and **B** with the laser power adjusted to yield the same initial steady-state intensity. Adapted from [29]

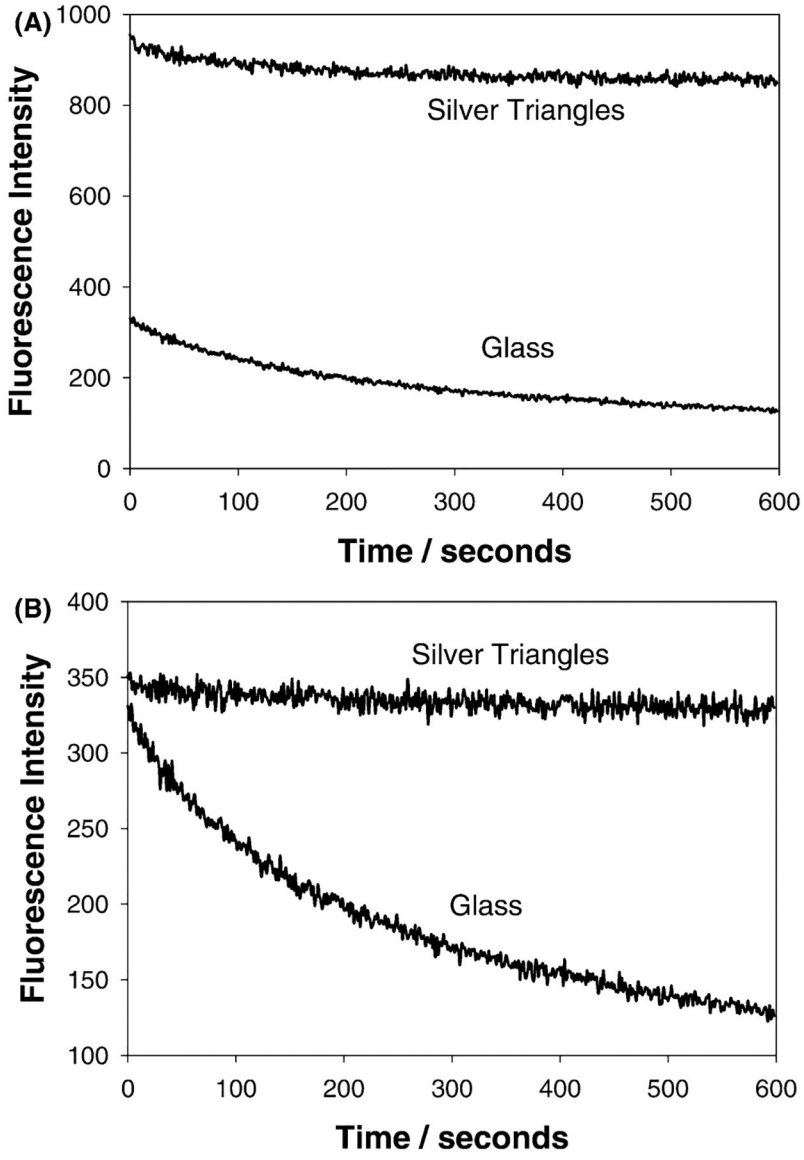

Fig. 11A–B.

A Photostability of ICG–HSA on silver triangular nanoplates prepared by the rapid deposition method, and **B** with the laser power adjusted to yield the same initial steady-state intensity. Adapted from [30]

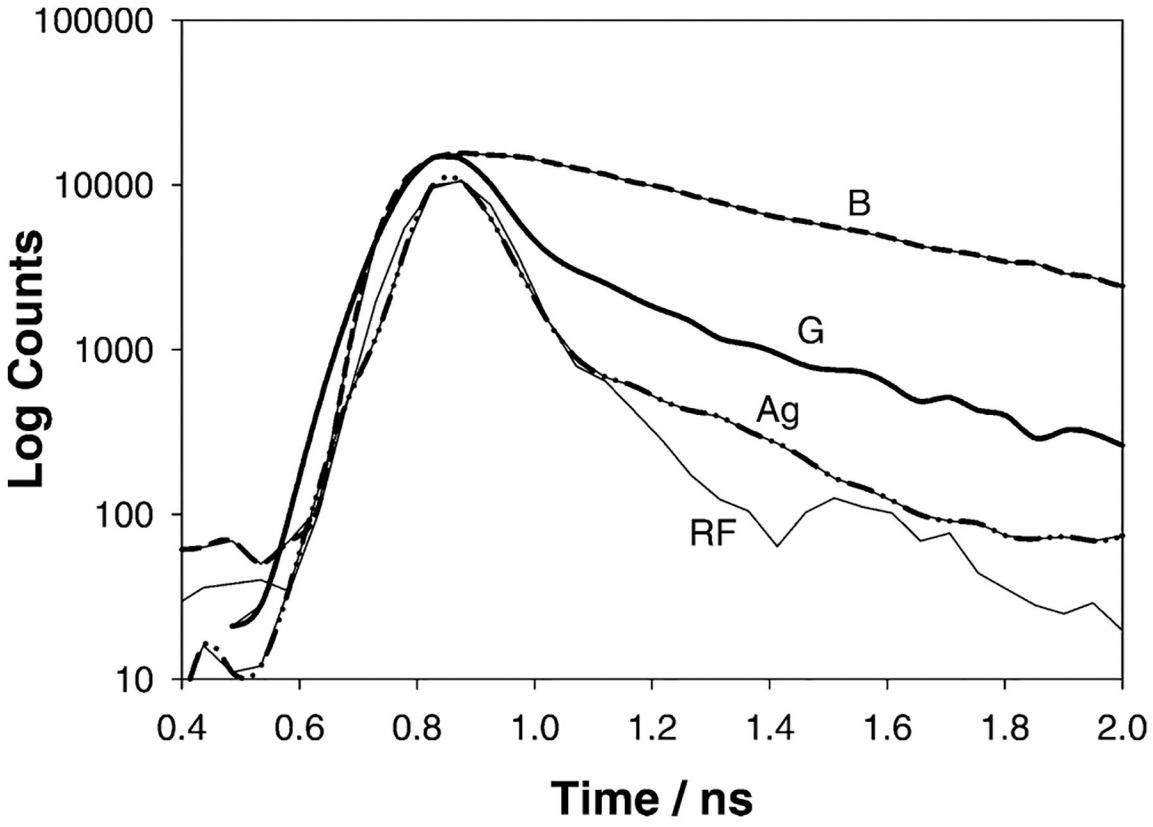

Fig. 12.

Complex intensity decays of ICG–HSA in buffer (*B*), deposited on glass slides (*G*), and on silver nanorods deposited by the fast deposition technique (*Ag*). The *RF* denotes the instrumental response function

Table 1

Multiexponential intensity decay of ICG–HSA on silver nanorods, deposited by the fast deposition method

Sample	$\tau_{1,2,3}$ (ns)	$a_{1,2,3}$	$\bar{\tau}$ (ns)	$<\tau>$ (ns)	χ^2
In buffer					
	0.190	0.158	0.592	0.548	1.4
	0.615	0.842			
On glass					
	0.233	0.558	0.645	0.484	1.4
	0.792	0.442			
Silver nanorods					
	1.070	0.008	0.412	0.023	1.7
	0.181	0.004			
	0.014	0.988			

τ lifetime, a amplitude, $\bar{\tau}$ mean lifetime, $<\tau>$ amplitude weighted lifetime